Electronic Supplementary Material (ESI) for Journal of Materials Chemistry C.


# Supplementary Information

## Quantitative Analysis of Improved Bending Fracture Behavior of Large-Scale Graphene Monolayer-Intervened Flexible Oxide Thin Films

Hong Je Choi [a,‡], Da Bin Kim [a,‡], Moo Hyun Kim [a], Gwan-Hyoung Lee [a], Yong Soo Cho[a,*]

[a]Department of Materials Science and Engineering, Yonsei University, Seoul 03722, Korea

*Corresponding author: ycho@yonsei.ac.kr (Y.S.Cho)
‡These authors contributed equally.

## 1. Detailed procedure of graphene transfer and deposition of ZnO:Al films

For the fabrication of the AZO/G/PET (Al-doped ZnO/graphene/polyethylene-terephthalate) structure, a monolayer graphene film was transferred onto the flexible polymer substrate by a peel-off transfer method prior to the ZnO:Al film deposition. The detailed processing steps to prepare the AZO/G/PET structure are schematically seen in Figure S1 below.

Commercially available monolayer graphene (1 cm x 1 cm, Graphene Supermarket, Reading, MA, USA) on a $SiO_2$/Si wafer was used here. For the initial spin-coating of polystyrene (PS) as a temporary adhesive layer, a 1.5 g PS pellet (molecular weight $M_w$ of ~192,000, Aldrich, St. Louis, MO, USA) was dissolved in 20 ml toluene via vigorous stirring. This solution was spin-coated at 1,000 rpm for 60 s on the graphene/$SiO_2$/Si and then heat-treated at 85 °C for 1 h. As the second layer, a polydimethylsiloxane (PDMS; Sylgard 184, Dow Corning Corp., USA) precursor mixed with a curing agent was degassed in a vacuum desiccator to remove air bubbles after manually stirring for at least 15 m. The ~50 μm-thick PDMS support layer was prepared by spin-coating at 3000 rpm for 90 s on the PS/graphene/$SiO_2$/Si and then by curing at 100 °C for 30 m.


**Fig. S1.** Schematic illustration of detailed processing steps for preparing the AZO/graphene/PET samples by a transfer technique of monolayer graphene

The sample was immersed in a deionized water bath so that the PDMS/PS/graphene stack could be removed from the $SiO_2$/Si wafer. The stack was safely scooped out onto the 175 μm-thick PET substrate while it was floated on the water's surface. To eliminate the PDMS stamp, the PS edge regions were partially decomposed by dripping toluene. Therefore, the

PDMS stamp was easily peeled off. For the complete removal of polymer residues, the graphene film on the PET substrate was rinsed with toluene and acetone for 2 h each.

A 2 wt.% Al-doped ZnO target (99.995% purity, CERAC Inc., Milwaukee, WI, USA) was used for the RF-magnetron sputter deposition of the corresponding films of ~50–200 nm thickness at room temperature. The distance between the target and the substrate was maintained at ~10 cm. The deposition was carried out at a constant RF power of 100 W at 13.56 MHz in a pure Ar atmosphere after the evacuation to a base pressure of ~5 x $10^{-6}$ Torr. The flow of Ar gas and the working pressure were respectively adjusted to 65 sccm and 2 mTorr. Predominantly c-axis-oriented AZO thin films were obtained with a hexagonal wurtzite structure.

## 2. The calculated applied strain values according to Eq. (1) given in text.

**Table S1**. Applied strains calculated for various film thicknesses as a function of bending radius in the case of no graphene intervention

| Bending radius (mm) | Applied strain (%) for various film thickness | | |
|---|---|---|---|
| | $t_f$=50 nm | $t_f$=100 nm | $t_f$=200 nm |
| 10 | 0.945 | 0.972 | 0.986 |
| 9 | 1.050 | 1.080 | 1.095 |
| 8 | 1.182 | 1.215 | 1.232 |
| 7 | 1.350 | 1.388 | 1.408 |
| 6 | 1.576 | 1.620 | 1.643 |
| 5 | 1.891 | 1.944 | 1.971 |
| 4 | 2.363 | 2.430 | 2.464 |
| 3 | 3.151 | 3.240 | 3.286 |
| 2 | 4.727 | 4.859 | 4.929 |
| 1 | 9.453 | 9.719 | 9.857 |

## 3. Optical transmittance and electrical resistivity of AZO thin films with graphene

We measured optical transmittance and electrical resistivity of the AZO films with and without graphene interlayer. As shown in Fig. S2, the effect of the graphene intervention was not significant. The slightly lowered transmittance of both the 50 nm and 200 nm-thick AZO samples were observed in the visible wavelength range by adopting the graphene layer. As expected, the AZO samples exhibited promising transparency of >~80%.

The electrical resistivity of the AZO samples, which were measured by a four-point probe

technique at room temperature, also indicates the least effect of graphene on the electrical properties of the AZO films. Very similar values were observed even with the graphene layer. It is noticeable that the thicker AZO film induced a lower electrical resistivity.

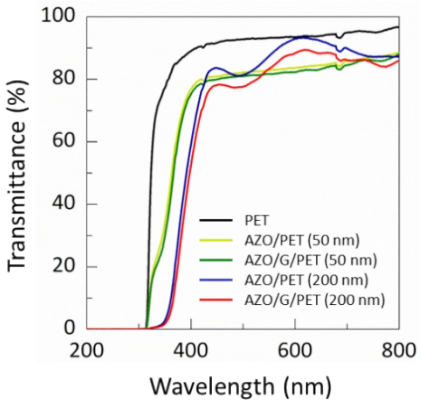


| **Electrical resistivity** | $t_f$=50 nm | $t_f$=200 nm |
|---|---|---|
| AZO | 0.0356 Ωcm | 0.0091 Ωcm |
| AZO/G | 0.0357 Ωcm | 0.0097 Ωcm |

**Fig. S2**. Transmittance curves of 50 nm and 200 nm-thick AZO/G/PET samples, with the electrical resistivity values measured at room temperature in a table on the right side

## 4. Cross-sectional SEM images

We double-checked the interface regions by observing the cross-sectional SEM images as shown in Fig. S3. There was no interfacial crack (or any detectable difference) at the interface when the graphene layer was intervened.

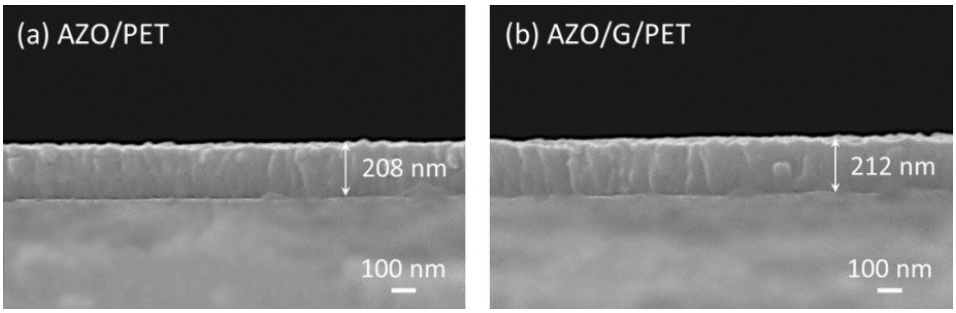


**Fig. S3**. Cross-sectional SEM images of AZO film grown (a) without and (b) with the graphene monolayer film (The samples were soaked in liquid nitrogen for 20 min to minimize plastic deformation of the polymer substrate for the sample preparation)

## 5. Bending fracture evaluation

The sample was loaded between two parallel holders and was gradually bent into a sinusoidal shape, thus exposing films to a tensile stress, with an applied force provided by a micrometer, as shown in Fig. S4. The cracking behavior around the center region of the sample by the bending test was recorded by *in situ* optical microscopy and expressed in terms of the number of cracks generated at a given strain.

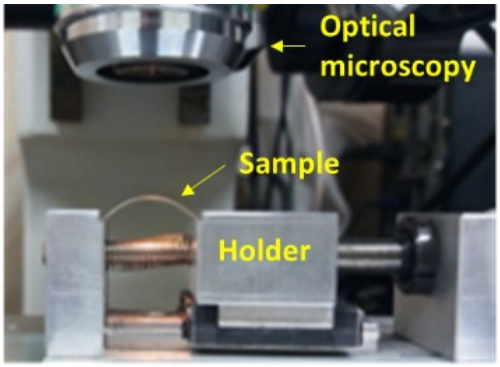


**Fig. S4**. A photograph of the testing set-up for the in situ measurement under bending operation of the flexible samples by using an optical microscope positioned directly on the top of the sample

## 6. Bending fracture images obtained by optical microscopy

Extensive optical images in Fig. S5 show the linear cracks that are developed onto the top of the AZO film surfaces depending on the applied uniaxial bending strain. The images were recorded by the *in situ* optical microscopy. It clearly demonstrates the effects of graphene-intervention and the thickness of AZO thin films on the evolution of cracks.

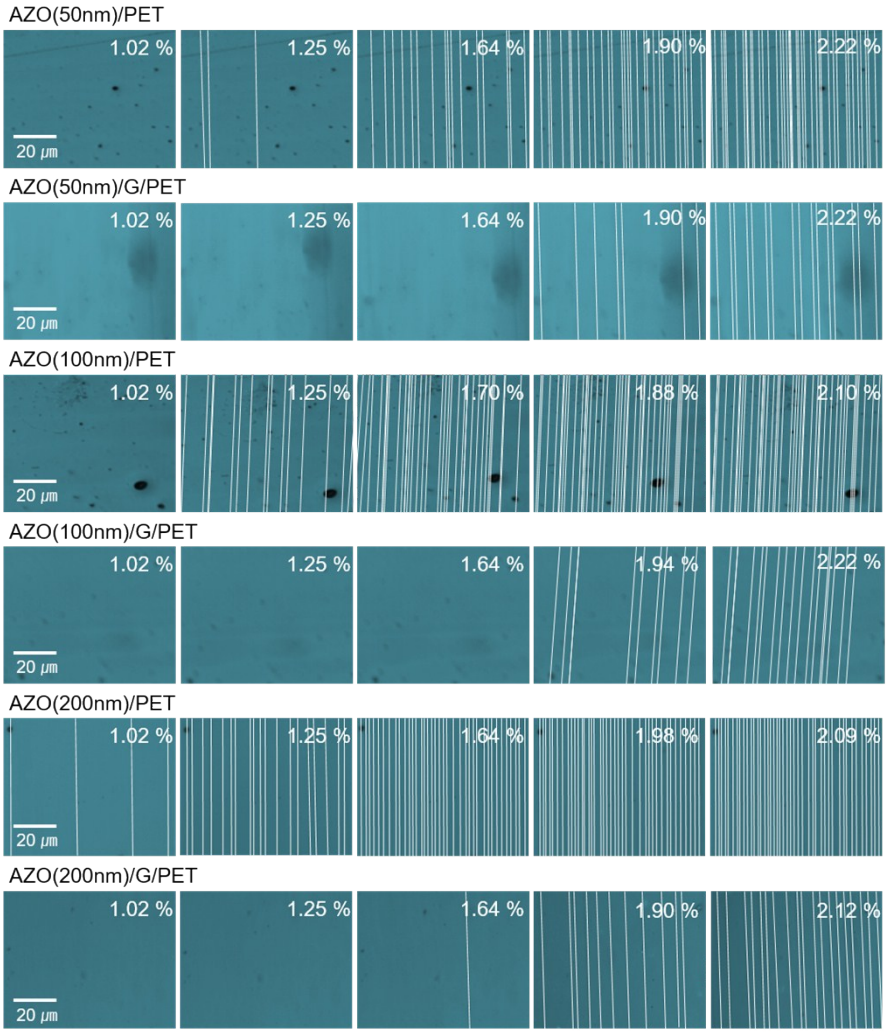


**Fig. S5.** Optical micrographs showing the evolutions of cracks in the flexible film structure of AZO/PET and AZO/G/PET with the variable film thickness of AZO from 50 nm to 200 nm. The increased density of cracks are clearly seen with increasing applied bending strains for all the cases.

## 7. Fracture SEM images

Fig. S6 shows the surface microstructures of the AZO/PET and AZO/graphene/PET samples after bending testing. The linear cracks perpendicular to the direction of bending are clearly seen. However, there is no difference in microstructure features around the evolved cracks between the two samples, which may indicate that the fracture mechanism itself may not be different regardless of the existence of graphene. It seems that the existence of graphene retards only the crack initiation by absorbing the external (bending) stress up to a certain level of strain.

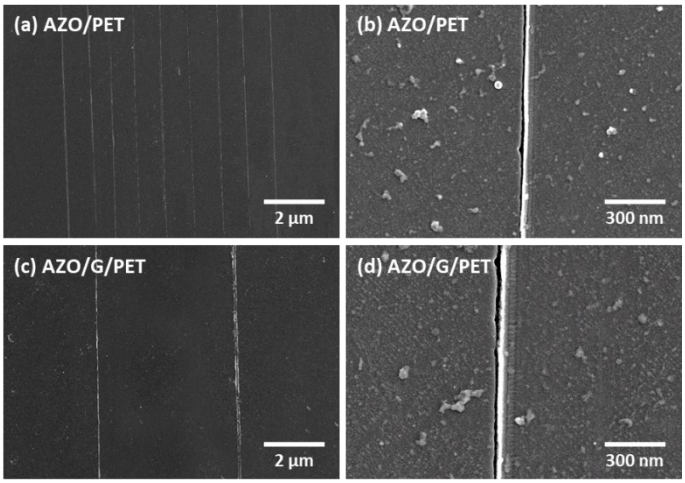


**Fig. S6**. Surface SEM photographs of the fractures AZO films showing the fracture behaviors in the cases of (a,b) no graphene and (c,d) graphene –intervention: the images of (b,d) correspond to the magnified ones around the linear crack for each sample.

## 8. Quantitative values of bending fracture behavior

**Table S2.** Bending fracture values of AZO/PET and AZO/G/PET samples with various AZO film thicknesses

| Mechanical parameters | AZO (200 nm) | AZO (100 nm) | AZO (50 nm) | AZO/G (200 nm) | AZO/G (100 nm) | AZO/G (50 nm) |
|---|---|---|---|---|---|---|
| Critical strain [%] | 1.02 | 1.13 | 1.28 | 1.64 | 1.71 | 1.75 |
| Saturated crack density [$\mu m^{-1}$] | 0.57 | 0.46 | 0.39 | 0.26 | 0.24 | 0.21 |
| Saturated crack spacing [μm] | 1.75 | 2.17 | 2.56 | 3.80 | 4.20 | 4.79 |
| Fracture energy [$Jm^{-2}$] | 98.0 | 143.2 | 213.9 | 364.2 | 409.6 | 445.5 |
| Fracture toughness [MPa $m^{0.5}$] | 3.84 | 4.63 | 5.67 | 7.39 | 7.84 | 8.18 |
| Film strength [MPa] | 148.0 | 163.9 | 185.7 | 237.9 | 247.8 | 253.6 |

## 9. Estimation of the $\beta$ value for the calculation of the fracture energy

In the energy criterion, film cracking can occur when the strain energy is higher than the required energy for crack nucleation at the critical strain. The fracture energy $\Gamma$ can be expressed in terms of $\alpha$ and $\beta$, as mentioned in the main text, which can be obtained from the relationship between the applied bending strain and the crack density, under an

approximation of the absence of mismatched strain. In addition, they can be given by[1–3]

$$\frac{\varepsilon_a}{\varepsilon_c} = \sqrt{\frac{3}{2f}} \tag{S1}$$

Where

$$f = 4\tanh\left(\frac{\alpha l}{2}\right) - \frac{e^{\alpha l} - e^{-\alpha l} + 2e^{\alpha l}}{e^{\alpha l} + e^{-\alpha l} + 2} - 2\tanh(\alpha l) + \frac{1}{2}\frac{e^{2\alpha l} - e^{-2\alpha l} + 4e^{\alpha l}}{e^{2\alpha l} + e^{-2\alpha l} + 2} \tag{S2}$$

here, $l$ is the term related to the crack density ρ, which can be obtained through the relationship $l = 2/3\rho$. Figure S7 shows the variation of the calculated and experimental $f$ values of non-intervened and graphene-intervened AZO/PET thin films with increasing applied bending strain. The calculated values agreed well with the experimental results when $\beta = 32$ and 11.2 for the AZO/G/PET and AZO/PET thin films, respectively.

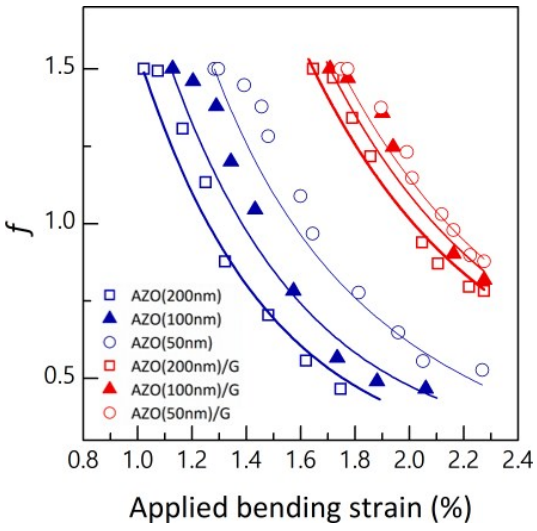


**Fig. S7**. Plots of $f$ as a function of the applied bending strain

References
(1) H. R. Choi, B. C. Mohanty, J. S. Kim, Y. S. Cho, *ACS Appl. Mater. Interface.* 2010, **2**, 2471-2474.
(2) C. H. Hsueh, M. Yanaka, *J. Mater. Sci*. 2003, **38**, 1809-1817.
(3) C. H. Hsueh, A. A. Wereszczak, *J. Appl. Phys.* 2004, **96**, 3501-3506.